ORCA – Online Research @ Cardiff

Citation for final published version:

Wu, Zhangming , Li, Hao and Deng, Zehua 2023. A novel design of vibration isolator with high and frequency dependent damping characteristics based on a Large Negative Poisson’s Ratio (LNPR) structure. Mechanical Systems and Signal Processing 186 , 109818. 10.1016/j.ymssp.2022.109818

Publishers page: https://doi.org/10.1016/j.ymssp.2022.109818

A novel design of vibration isolator with adaptive damping characteristics based on negative Poisson's ratio metastructures

Zhangming Wu[a,c], Hao Li[b], Zehua Deng[b]

[a]*School of Mechanical Engineering and Mechanics, Ningbo University, Ningbo 315211, Zhejiang Province, China*
[b]*Shanghai Institute of Satellite Engineering, Shanghai, China*
[c]*Cardiff School of Engineering, Queens Buildings, The Parade, Newport Road, Cardiff CF24 3AA, UK*

Abstract

In this paper, a biconcave-lens shaped metastructure unit cell with a large value of negative Poisson's ratio (NPR) is designed and analyzed. By filling viscoelastic damping materials inside in this metastructure, a novel vibration isolator with adaptive damping characteristics is designed and analyzed. The advantage of this novel design of vibration isolator is that its high damping characteristics for the low-frequency vibration isolation can be achieved in a small volume without affecting its high-frequency vibration isolation effect. The negative Poisson's ratio of the metastructure causes its amplified lateral deformation, which will then lead the inside filled viscoelastic materials to have enlarged compression or tension along the lateral direction during the vibration process. As a consequence, the viscoelastic materials can effectively dissipate energy, thereby improving the damping characteristics and the overall performance of the vibration isolator. Finite element simulation is performed to predict the static and dynamic characteristics of the negative Poisson's ratio vibration isolator, and characterize the hyperelastic and viscoelastic properties of the damping rubber. Finally, a vibration isolation platform based on four negative Poisson's ratio vibration isolators is designed and installed for the frequency-sweep testing to prove our proposed negative Poisson's ratio vibration isolator.

---

*Corresponding author
Email address: `shsehaoli@126.com` (Hao Li)

Keywords: vibration isolator, metastructure, negative Poison's ratio, viscoelastic damping

---

1. Introduction

High-precision instruments and devices [1] play an increasingly important role in many science and technology fields, e.g. precision machining and manufacturing, microelectronics, optical imaging, precision positioning, biology detection, and space structures etc [2, 3, 4, 5, 6]. Micro-vibrations are generated either from external working environment or internal driving (rotating) elements often disturb the accuracy, performance or even normal operation of high-precision instruments [7]. Herein, the micro-vibration refers to low-amplitude vibration with frequency up to 1 kHz [8]. Developing an isolation system that can largely and effectively suppress micro-vibrations is essential to prevent the instruments being disturbed and further increase their accuracy. To meet the increasing precision standards in industry, there remains ongoing research interests to develop novel, effective, lightweight and small-size vibration isolation systems. This research aims to develop a metastructure based passive vibration isolator with adaptive damping characteristics, which can effectively suppress resonance amplitude and simultaneously maintain the vibration isolation effect at high-frequencies. To achieve this goal, a novel integrated use of the metastructure with negative Possion's ratio (elastic element) and viscoelastic materials (damping element) is proposed and designed in this work.

Compared with active control methods, passive vibration isolators can effectively reduce the structural response under dynamic loads [9]. Passive vibration isolator is one of the main approaches for structural vibration control at present. It has the advantages of low cost, reliable operation without additional energy consumption [5]. In general, a passive vibration isolator is composed of elastic elements and damping elements [10, 11]. The essence for the design of a passive vibration isolator is to properly design stiffness and damping elements. In particular, the damping element of a vibration isolator normally determines its resonance magnification and energy dissipation capacity [11], both of which are the key parameters affecting the vibration isolation performance. According to the energy dissipation principle, passive dampers can be divided into hysteresis, viscoelastic, mass damper, viscous, magnetic negative stiffness devices, and resetting passive stiffness devices, etc

[12]. Nevertheless, the design of elastic elements is usually uncomplicated, for which the volume and the weight of elastic elements can be effectively tailored using a structural optimization process. In order to reduce the resonance magnification of vibration isolators as much as possible, the energy dissipation capacity of the damping element should be designed to achieve a maximum. On the other hand, it is usually more complicated and difficult to control its volume and weight to achieve high damping coefficients for damping elements. For example, a fluid viscous damper requires a sealed cavity, piston and damping liquid to form a damping force, and there is a risk of liquid leakage [13]. A variety of different types of fluid viscous dampers have been developed for seismic isolation in bridges [13] or the micro-vibration isolation in satellites [4]. However, the complexity and large weight of fluid viscous dampers are often unavoidable. Mass dampers need the use of mass blocks and mass amplification mechanisms to achieve high damping characteristics [14]. Therefore, the design of mass dampers is also complicated and it is very difficult to achieve lightweight and minimization. Hysteresis dampers require large relative displacements to function [15], and are only suitable for the applications with large-amplitude vibrations, but are difficult to apply to micro-vibration isolation applications. Therefore, designing vibration isolation systems for high-precision instruments that requires high quality, lightweight within a limited volume is a very challenge task.

To design small, lightweight and high quality vibration isolation systems for precision instruments, the metamaterials and metastructures provide attractive solutions due to their small sizes, lightweight and extensively designable properties [16]. Metamaterials, which are constructed by artificially designed and additively manufactured structural architectures, can exhibit various distinct or unusual properties, such as high strength and stiffness at ultra-low weight [17], negative effective mass density [18], negative elastic stiffness [19], zero/negative Poisson's ratio [20, 21], and negative thermal expansions [22] etc. In recent years, many research works have designed various types of metamaterials that possess extraordinary capability of broadband vibration attenuations [23, 24]. One typical example is to use buckled/curved beams based unit cells acting as the negative stiffness elements in vibration isolators [25, 26]. Many further research works have developed various types of quasi-zero stiffness (QZS) isolators through designing particular unit cells with negative stiffness and assembling the unit cells in appropriate manners [24, 26, 27, 28]. The metamaterials based vibration isolators with the QZS properties and small sizes will be appropriate in the applications of precision instruments or microdevices [26]. Moreover, for the purpose of responsing the changes of external environment and working conditions, many programmable/tunable QZS vibration isolators with switching mechanical properties and vibration isolation effect are also developed based on 4D printing technology [21, 24, 29]. In particular, Wang *et al.* [30] proposed a tunable digital metamaterial to broaden the frequency range of bandgaps leading to the potentials of developing intelligent vibration isolation systems. Nevertheless, designing the vibration isolation capability of metamaterials solely based on their micro-structural architectures limits the potentials, in particular for exploring the advantageous damping mechanism.

Viscoelastic dampers that use viscoelastic materials for the energy absorption had been widely applied in the vibration control of many engineering fields, e.g., buildings, bridges, machinery and precision instruments [31, 32, 33, 34], due to its advantages of lightweight, simple form, low cost, and having no risks of leakage and performance degradation. After many years of development, there are three main forms for viscoelastic dampers, namely free layer damping, constrained layer damping and shear deformation damping [35, 36]. A large number of studies have shown that the energy dissipation effect of viscoelastic materials is much better when shear deformation occurs, as such, the shear deformation type is the most commonly used form for viscoelastic dampers [35, 36]. In engineering applications, a typical example of a shear-type viscoelastic damper is that a viscoelastic damper installed between the center pole of the solar wing and the Hubble Space Telescope (HST) [37]. The basic principle is to provide a viscoelastic material layer between rigid elements. When the relative displacement occurs between the rigid elements, the viscoelastic material layer will undergo shear deformation and dissipate energy. Although the shear deformation type viscoelastic damper has been approved to have excellent damping characteristics, its shortcomings are also very obvious [38]. Firstly, in order to achieve high energy dissipation characteristics, the thickness of the viscoelastic shear damping layer should be reduced as much as possible, and the area of the viscoelastic shear damping layer should be increased. As a result of small thickness and large area of the viscoelastic shear layer, the damper will have very large rigidity, and it is very difficult to suppress the vibration at low frequencies. Secondly, the viscoelastic shear damping layer needs to be bonded to the rigid part, which is not conducive to the lightweight design of the damper, and the integrated design of damper and elastic element becomes very difficult. Thirdly, due to the small amplitude of the micro-vibration, the shear strain of the viscoelastic material is too small to dissipate the vibration energy, effectively. Therefore, for the micro-vibration isolation, it is very necessary to magnify the shear strain of the viscoelastic material, whilst, in the meantime, suppress the vibration peak at the resonance frequency.

In summary, as a damping material, viscoelastic materials have simple structural forms and efficient damping characteristics, however, it is also necessary to combine it with a well-designed structural element to achieve proper damping characteristics. To meet the demands for micro-vibration isolation in precision instruments and devices, this paper proposes a novel vibration isolator with adaptive damping characteristics, lightweight and small size, by filling the viscoelastic materials into a negative Poisson's ratio elastic metastructure. With the finite element simulation, this paper first approves the basic design principle and working mechanism of this novel vibration isolators and its adaptive damping characteristics. Next, the energy dissipation characteristics, statics and dynamics characteristics of this novel vibration isolators are analyzed using both finite element simulation results and experimental testing results. Finally, a vibration isolation platform using four negative Poisson's ratio vibration isolators is designed and installed to carry out the frequency-sweep testing to further verify its vibration isolation effect.

2. Design and analysis of the metastructure unit cell

2.1. Design a unit cell with negative Poisson's ratio

Many previous research works of mechanical metamaterials have shown that, with an appropriate design of microstructures, an elastic structure can exhibit a negative Poisson's ratio (NPR) macroscopically, which is an useful feature applying for vibration isolation [39, 40]. Inspired by many previous designed mechanical metamaterials and metastructures, a basic structural unit cell with negative Poisson's ratio for vibration isolators is first designed in this paper, as shown in Fig. 1. The metastructure is composed of a biconcave-lens shaped structure, which naturally exhibits a negative Poisson's ratio and will be filled with damping rubber materials inside. The negative Poisson's ratio property for this metastructure is achieved due to the two inwardly arc-shaped sheets, which will deform laterally when they are compressed or stretched longitudinally. When the two arc sheets are stretched longitudinally, their lateral spacing will expand, whilst when they are compressed longitudinally, their lateral spacing will shrink. Therefore, the entire structure exhibits a negative Poisson's ratio property.

When the initial bending curvature of the arc-shaped sheet is properly designed, the transverse deformation of the arc-shaped sheet will be much greater than its longitudinal deformation, and the absolute value of the Poisson's ratio for this structure can be greater than 1. When the negative Poisson's ratio structure produces longitudinal tension and compression, the enlarged lateral deformations of the arc sheets make the internally filled damping rubber material effectively squeezed or stretched along the lateral direction, which in turn increases the overall damping ratio of this metastructure.

2.2. Modelling and testing of the metastructure unit cell

The finite element model is built to simulate and study the deformation characteristics of the negative Poisson's ratio structure. The negative Poisson's ratio structure is modeled by shell elements S4. The geometry and the dimensions are shown in Fig. 4(a). In the finite element analysis, the length of the negative Poisson's ratio structure is set as $l = 40$mm, the width $w = 20$ mm, and the height $h = 10$ mm. The length l, width w and height h are denoted in Fig. 4. In the follow-up experiment, a prototype of this biconcave-lens shape based metastructure is fabricated by a 3D printer. The material used in 3D printing is PLA plastic ($E = 3$ GPa, $\mu = 0.3$), and the diameter of the nozzle of the 3D printer in this experiment is 0.4 mm. Therefore, the thickness of the arc-shaped sheet is $t = 0.8$ mm, which equals the thickness of the two layers of materials. After fixing the bottom of the metastructure and applying a vertically displacement-controlled load on the top, the simulation curve that represents the lateral deformation at the center of the metastructure with respect to the vertical deformation is plotted and shown in Fig. 4. The results of the finite element analysis show that the lateral deformation at the center of the metastructure is much larger than its vertical deformation under the vertical tensile or compressive loads. When the chord height Δh of the arc-shaped sheet is decreased, the lateral deformation at the center of the metastructure will be increased, resulting in more obvious nonlinear characteristics in the curve of the lateral deformation *vs.* the vertical deformation of metastructure.

In order to verify the finite element model of this NPR metastructure, an experimental testing is carried out on a 3D printer fabricated prototype, as shown in Fig. 5(a). After obtaining the experimental results from the standard mechanical testing, the curve of longitudinal tensile force *vs.* vertical displacement for this NPR metastructure is plotted, as shown in Fig. 5(b).

The experimental curve matches very well with the finite element simulation results. It also shows that this NPR metastructure exhibits a nonlinear structural behaviour. Fig. 5(b) also shows that this NPR metastructure possesses increasing longitudinal stiffness with the increase of tension force (positive values of Load in Fig. 5(b)), and decreasing stiffness with the increase of compression force (negative values of Load in Fig. 5(b)).

2.3. Damping materials

Because the stress of viscoelastic material lags behind the strain, it can effectively dissipate energy during the vibration process and can act as a damping element in a vibration system. In this paper, butyl rubber is adopted as the damping material of the vibration isolator. Butyl rubber has high dynamic stiffness and low static stiffness, and has obvious creep characteristics under static load. In this paper, ABAQUS is used to simulate viscoelastic materials, for which the properties of hyperelastic materials are adopted. The 2-parameter Mooney-Rivlin model is applied to model the hyperelastic materials, and the prony series are used to characterize the viscoelastic properties of the material. The viscoelastic material parameters in the simulation are shown in Table 1. The Mooney-Rivlin model parameters given in Table 1 are fitted using the experimental testing results, which will be discussed in Section 3.1. Fig. 2 shows the force-displacement curve of a viscoelastic material with a volume of 10 mm cubic under periodic stretching. Based on the material properties in Table 1, the stress-strain curve and shear relaxation curve of the viscoelastic material are shown in Fig. 3. The force-displacement curve of the viscoelastic material in Fig. 2 forms a closed loop, and the area of the closed loop is the energy consumed by the viscoelastic material in one vibration cycle. The analysis results of different vibration rates in Fig. 2 show that the energy dissipation characteristics of viscoelastic materials are related to the loading rate. The energy dissipated by a viscoelastic material per cycle when vibrating at low frequencies is significantly greater than the energy dissipated per cycle when vibrating at high frequencies. Therefore, when viscoelastic materials are used as damping elements, their damping ratios will gradually decrease as the vibration frequency increases. For a vibration isolation system, the ultimate design goal is to have high damping ratios at low frequencies to reduce the magnification of the vibration isolation system at the resonance frequency, and at the same time, to have lower damping ratios at high frequencies to improve the vibration isolation efficiency, namely *adaptive* damping characteristics. Therefore, the viscoelastic materials with the damping ratios that are decreasing with the increase of frequency are the ideal damping materials for vibration isolation systems.

When a viscoelastic material is used as the damping material in a single degree of freedom vibration isolator, the simplest design is that the elastic element and the viscoelastic material in the vibration isolator are connected in parallel. For the micro-vibration isolation of precision instruments, because the vibration magnitude is usually in the micron-meter level, it is difficult for viscoelastic materials to produce sufficient deformation. As a result, the deformation will mainly be elastic deformation, and its viscoelastic energy dissipation capacity is difficult to be fully exerted. When the pure shear deformation of viscoelastic materials is used for the main energy consumption mechanism [41], the thickness of the viscoelastic damping layer must be made as small as possible, so as to achieve great shear strain in a micro-vibration environment. However, a smaller thickness of the damping layer will cause the shear dynamic stiffness of the damping layer to become too large, and the shear deformation of the damper will decrease under the same vibration excitation. Furthermore, if the dynamic stiffness is too high, it will affect the vibration isolation efficiency of the vibration isolator. For the micro-vibration isolation of precision instruments, in order to increase the energy dissipation capacity of viscoelastic materials, it is necessary to increase the amount of deformation of viscoelastic materials during the vibration process. Therefore, in this paper, a viscoelastic material is directly embedded into a NPR elastic element, in doing so, the deformation of the viscoelastic material is amplified through the NPR effect of the elastic metastructure to achieve high damping characteristics.

3. Finite element analysis of the high damping vibration isolator

In order to achieve high damping characteristics for the vibration isolator, in this work, the above designed NPR metastructure is filled with uncured butyl rubber, as shown in Fig. 1. The uncured butyl rubber used herein is mixture from butyl rubber, polyisobutylene and other raw materials, which have self-adhesive and good elongation properties. Hyperelastic elements C3D8RH (An 8-node linear brick element using reduced integration with hourglass control, and hybrid with constant pressure) are used to model the butyl rubber in the finite element model for the vibration isolator. The hyperelastic element is based on the 2-parameter Mooney-Rivlin model [42],

$$W = C_{10}(\bar{I}_1 - 3) + C_{01}(\bar{I}_2 - 3) + \frac{1}{D_1}(J-1)^2 \tag{1}$$

where W is the strain energy per unit of reference volume, and C_{10}, C_{01}, D_1 are temperature-dependent material parameters; $\bar{I}_1$ and $\bar{I}_2$ are the first and second deviatoric strain invariants. The instantaneous elastic modulus of butyl rubber is 4.5 MPa. We assume that the material parameters $C_{10} = 4C_{01}$[43], and $6(C_{10} + C_{01}) = 4.5$ MPa, the material parameters C_{10} and C_{01} can be easily determined. The material parameters D_1 is determined by $D_1 = 1/\left(2(C_{10} + C_{01})\right)$. The obtained material parameters C_{10}, C_{01}, D_1 are presented in Table 1. Butyl rubber is a viscoelastic material, and its mechanical response is related to the deformation rate and time. In Abaqus model, the time-varying shear stress of a viscoelastic material is expressed as,

$$g_R(t) = G_R(t)/G_0 \tag{2}$$

where $g_R(t)$ is the dimensionless shear relaxation modulus, $G_R(t)$ is the shear relaxation modulus, and G_0 is the instantaneous shear modulus. The expression for the stress takes the following form as,

$$\tau(t) = G_0 \int_0^t g_R(t-s)\dot{\gamma}(s)ds \tag{3}$$

In this paper, we use the prony series to define the dimensionless shear relaxation modulus as,

$$g_R(t) = 1 - \sum_{i=1}^{N} \bar{g}_i^P \left(1 - e^{-t/\tau_i^G}\right) \tag{4}$$

where N, $\bar{g}_i^P$, τ_i^G $(i = 1, 2, \cdots, N)$ are material constants. $N = 3$ is selected in the finite element simulation. In order to obtain the parameters g_i, k_i and τ_i, we used a tensile testing machine to measure the hysteresis curve of this proposed vibration isolator, and adjust the parameters g_i, k_i and τ_i according to the hysteresis curve. The obtained parameters are presented in Table 1. In the test, the vibration isolator was loaded cyclically at a uniform speed, and the loading rates were 1mm/min and 20mm/min, respectively. Based on the parameters provided in Table 1, the comparison between the hysteresis curves of the vibration isolator obtained by the finite element simulation and that given by the experimental testing is shown in Fig. 6. It can be seen that the finite element model can accurately reproduce the experimental testing results for the hysteresis curve of the vibration isolator. Both finite element simulation and experimental testing show that the vibration isolator as a whole has obvious hysteretic damping characteristics. Fig. 7 compares the deformations of the same shape butyl rubbers within and without the NPR metastructure, respectively, when they are under longitudinal tension and compression loads. Under the longitudinal tension and compression, the butyl rubber with the NPR metastructure is further compressed and stretched due to the effect of the negative Poisson's ratio along the transverse direction. As a result, the lateral deformations of the butyl rubber within the NPR metastructure are approximately 10 times of that of the butyl rubber under free stretching state.

Superelastic	C_{10}	C_{01}	D_1
	600000	150000	8e-8
Viscoelastic	g_i	k_i	τ_1
	0.935	0	0.01
	0.0487	0	1
	0.0162	0	20

Table 1: Superelastic and viscoelastic model parameters of the butyl rubber in the finite element simulation

The energy consumption of the vibration isolator under cyclic loading at different frequencies is analyzed using the finite element model, and is compared with that of the butyl rubber under freely deforming state (unrestrained). A sinusoidal function based longitudinal displacement cyclic loading $d = 0.5\sin(2\pi ft)$mm is applied to the vibration isolator and the unrestrained rubber. The creep dissipation energies of both the high damping vibration isolator and the unrestrained rubber after 3 cyclic loadings are obtained and shown in Fig. 8. Under different cyclic loading frequencies, the creep loss energy of both the high damping vibration isolator and the unrestrained rubber varies in the same trend. However, the creep dissipation energy of each cycle of the damping rubbers (both within the vibration isolator and under the unrestrained state) in the low-frequency vibration process is greater than the creep dissipation energy of each cycle in the high-frequency vibration. In the vibration isolator, due to the large lateral deformation of the damping rubber with the constraint of the NPR metastructure, the creep dissipation energy of the damping rubber in the vibration isolator is much greater than that of the damping rubber under unrestrained state at all frequencies. From the results shown in Fig. 8, it approves that the NPR metastructure based vibration isolator proposed in this paper exhibits much higher damping characteristics during the vibration process compared with the conventional vibration isolator in which the elastic element and the damping rubber are simply connected in parallel.

4. Dynamic characteristics of the vibration isolator

In order to study the vibration isolation effect of the proposed vibration isolator, its free vibration behaviour is first analyzed using the finite element model. The obtained numerical results are compared with the conventional vibration isolator using the same damping rubber and the spring with the same elastic stiffness. The prototypes for the finite element model of the NPR metastructure based vibration isolator and the conventional vibration isolator are illustrated in Fig. 9(a). In the finite element model, a coupling constraint is set between the top of the vibration isolator and a reference point, and the inertial mass is set at the reference point. In order to simulate the conventional vibration isolator with linear spring and damping rubber, the spring connection is directly used in the finite element model to simulate the linear spring, and the end of the linear spring is coupled with the damping rubber. If the inertial mass on the top of the NPR vibration isolator is set to 10 kg, the fundamental frequency of the vibration isolator is 44.2 Hz, which is predicted by the finite element simulation. If the stiffness of the linear spring is set to 755000 N/m, the fundamental frequency of the linear spring isolator is identical with that of the NPR vibration isolator, i.e. 44.2 Hz. For the finite element simulation process: (1) Firstly, the bottoms of these two kinds of vibration isolators are fixed; (2) Next, an initial vertical displacement is applied to the inertial mass point on the top of each vibration isolator using a static analysis step; (3) Subsequently, the displacement constraint of the mass point is released in an implicit dynamic analysis step, with which the free vibration of the mass point is analyzed. The free vibration analysis results for the linear spring vibration isolator and the NPR vibration isolator are obtained and shown in Fig. 9(b). The analysis results clearly approve that, with the use of same damping rubbers, the damping characteristic of the NPR metastructure based vibration isolator is significantly better than that of the linear spring vibration isolator.

Since the damping rubber is a non-linear material and the NPR metastructure is a variable stiffness structure, in order to analyze the vibration isolation effects of the NPR vibration isolators and the linear spring vibration isolator at different frequencies, implicit dynamics analysis is carried out. The analysis step analyzes the response of the two types of vibration isolators using a sweep frequency excitation. In order to simulate the sinusoidal sweep frequency excitation with constant acceleration, the excitation wave is generated using Eq. (5), with which tabular values for the excitation amplitude and frequency are computed and applied for the implicit dynamics analysis using the tabular amplitude function (Tabular Amp) in ABAQUS.

$$\text{Amp} = \begin{cases} \frac{0.1t}{(40\times 2\pi)^2} \times \sin(40 \times 2\pi t), & t = 0 \sim 5s \\ A \sin\left(2\pi \int 40 \times 2^{\frac{t-s}{60}} R dt\right) & t = 5 \sim 65s \end{cases} \tag{5}$$

where A is the amplitude of acceleration, $A = 0.1$ m/s^2, R is the frequency sweep rate, $R = 2$ otc/min. t represents the time that the implicit kinetic analysis step takes. When the excitation acceleration is set to 10 mg (the unit mg denotes micro stand gravity, 1 mg $= 0.001 \times 9.8$ m/s^2), the acceleration excitation curve generated by Eq. (5) is shown in Fig. 10. In the first 0 to 5 seconds of the frequency sweep process, the excitation frequency remains unchanged at 40 Hz, and the excitation amplitude linearly increases from 0 to 10 mg; in the next 5 to 65 seconds, the excitation amplitude remains unchanged at 10 mg, and the excitation frequency is changed from 40 Hz to 160 Hz with an increasing speed of 2 otc/min.

Under the excitation that is shown in Fig. 10, the acceleration response results of the two types of vibration isolators (as given in Fig. 9) installed with two different inertial masses of 10 kg and 3.3875 kg are predicted using the finite element analysis, and the data curves are presented in Fig. 11. The results clearly show that, at the resonance amplitude, the vibration amplitude of the linear spring vibration isolator is much greater than that of the NPR vibration isolator. Moreover, the response curve for the linear spring vibration isolator exhibits an obvious beat phenomenon near the resonant peak. When different masses are installed on the top of the vibration isolator, the peak response amplitudes and the corresponding frequencies of the two types of vibration isolators are compared and presented in Table 2. The damping characteristics of the NPR vibration isolator near the resonance frequency is much greater than that of the linear spring vibration isolator. When the excitation frequency is increased up to 160 Hz, the acceleration response curves for the two vibration isolators almost completely overlap. It indicates that, under high frequency excitation, the damping characteristics of the NPR vibration isolator are almost the same with those of the linear spring vibration isolator. When the masses are 10 kg and 3.3875 kg, the resonance frequency analysis results of the NPR vibration isolator under 10 mg excitation are 43.7 Hz and 74.2 Hz, respectively. For a single degree of freedom undamped vibration isolator with the resonance frequencies of 43.7 Hz and 74.2 Hz, the vibration transmission rate is computed by,

$$T_{UD1DOF} = 20\log_{10}\left[\sqrt{\frac{1}{\left(1-\left(\frac{f}{1/f_{resonance}}\right)^2\right)^2}}\right] \tag{6}$$

where f is the excitation frequency, and $f_{resonance}$ is the resonance frequency of the single-degree-of-freedom undamped vibration isolator. The vibration transmission rate of the NPR vibration isolator for the frequency response curves shown in Fig. 11 is computed via,

$$T_{NPRVI} = 20\log_{10}\left[(a_{response})/(10\text{mg})\right] \tag{7}$$

where $a_{response}$ is the response acceleration of the system with respect to the input excitation 10 mg. The vibration transmission rate of the NPR vibration isolator given by Eq. (7) is compared with that of the undamped single degree of freedom vibration isolator calculated by Eq. (6), as shown in Fig. 12. The comparison results in Fig. 12 clearly show that the vibration magnification of the NPR vibration isolator at the resonance frequency can be effectively suppressed, and the vibration transmission rate at the high frequency is the same with that of the undamped linear vibration isolator with the same stiffness. Therefore, this unique damping characteristics of the NPR high damping vibration isolator can effectively suppress its resonance magnification, but do not have any obvious effect on its high-frequency vibration isolation efficiency, namely achieving an *adaptive* damping characteristics.

5. Experimental testing of the vibration isolator

By applying 4 NPR high damping vibration isolators, a vibration isolation platform, as shown in Fig. 13, is designed, installed and tested in this paper.

	M=10kg		**M=3.3875kg**	
	LS Isolator	NPR Isolator	LS Isolator	NPR Isolator
Maximum Acceleration(mg)	943	91	1223	152
Resonance Frequency(Hz)	44.5	43.7	75.2	74.2

Table 2: Comparison of the Resonance Response between LS (linear spring) Isolator and NPR (Negative Poisson's Ratio) Isolator

The upper part of the vibration isolation platform is made of aluminum alloy thick plate, weighing 0.75 kg. The vibration isolation platform is placed on a large-scale shaking table, which is used to carry out the frequency-sweep testing and measure the vibration transmission rate of the vibration isolation platform. In the frequency-sweep testing, the frequency range is set to 15 Hz $\sim$ 300 Hz, and the sweep rate is chosen as 2 otc/min. In the testing, two different masses of 12.8 kg and 3.8 kg are placed on the vibration isolation platform, respectively. As such, the corresponding total mass of the top of the vibration isolators is 13.55 kg and 4.55 kg, respectively. In the test, the vibration isolator will be pre-compressed under the influence of the weight of the installed mass. In order to analyze the influence of gravity on the fundamental frequency of the vibration isolation platform, we first use the "*VISCO" step in ABAQUS to analyze the deformation of the vibration isolation platform. Since the damping rubber in the vibration isolator is a viscoelastic material, the deformation of the vibration isolator will increase nonlinearly with the increase of time and gradually become stable. The curve for the static compression deformation of the vibration isolation platform varying with respect to time is plotted and shown in Fig. 14. When the compression deformation of the vibration isolation platform is stabilized, the fundamental frequency of the vibration isolation platform is re-analyzed. The analysis results are presented in Table 3. It is observed that the fundamental frequency of the vibration isolation platform has dropped slightly.

Fig. 15 shows the vibration transmission rate curve when different masses are installed on the upper part of the vibration isolation platform. Table 4 presents the maximum vibration magnification and corresponding frequency under differently installed mass conditions. The experimental testing results show that the maximum magnification of the vibration isolation platform gradually decreases with the increase of the excitation amplitude. Under the

		Fundamental Frequency (Hz)	
		Total Mass = 13.55 kg	Total Mass = 4.55 kg
FEA	Without gravity	75.1	129.4
	With gravity	69.2	125.0
Experiment (Excitation = 10 mg)		70	124

Table 3: Numerical predictions and experimental testing results for the fundamental frequency of vibration isolation platform

influence of the nonlinear characteristics of the vibration isolator, when the installed mass is 13.55 kg, the resonance frequency of the vibration isolation platform gradually decreases with the increase of the excitation amplitude. Under 10 mg excitation, the corresponding frequencies at the resonant peaks of the vibration isolation platform with the 13.55 kg and 4.55 kg installed mass blocks are about 70 Hz and 124 Hz, respectively, which are consistent with the finite element analysis results, as shown in Table 3.

	Excitation Amplitude							
	10 mg		20 mg		30 mg		40 mg	
Total Mass	Mag.	Freq.	Mag.	Freq	Mag.	Freq.	Mag.	Freq.
13.55 kg	4.009	70 Hz	3.699	124 Hz	3.500	66 Hz	3.385	64 Hz
4.55 kg	4.179	124 Hz	4.149	124 Hz	3.971	124 Hz	3.786	124 Hz

Table 4: Maximum vibration magnification

In order to calculate the equivalent damping coefficient of the vibration isolation platform, the vibration isolation platform is simplified as a single degree of freedom vibration isolation system. The analytical solution of the vibration transmissibility of a single-degree-of-freedom vibration isolation system is [44],

$$\text{Transmissibility} = 20\log_{10}\left[\sqrt{\frac{k^2 + c^2\omega^2}{(k - m\omega^2)^2 + c^2\omega^2}}\right] \tag{8}$$

where k is the equivalent stiffness of the vibration isolation system, c is the equivalent damping coefficient, and ω is the angular frequency. In order to estimate the equivalent stiffness and damping coefficient of the vibration isolation platform, we first assume that the resonance frequency f of the vibration isolation platform without damping, with which the equivalent linear stiffness of the vibration isolation platform is given as $k = (2\pi f)^2 m$. Substituting the hypothetical value of k, the resonance frequency and amplification factor, which are obtained from the experimental testing, into Eq. (8), the equivalent damping coefficient can be determined by solving Eq. (8). For a linear vibration isolation system, when the damping coefficient c is large, the resonant peak of the damped vibration isolation system will shift to the left compared with the resonant peak of the undamped vibration isolation system. In other words, there is a slight decrease of the resonance frequency of the damped vibration isolation system under the influence of damping. When the installed masses are 13.55 kg and 4.55 kg, assuming that the resonance frequency f of the vibration isolation platform without damping is greater than the resonance frequency measured from the experimental testing, e.g., we take $f = 71.5$ Hz and $f = 126$ Hz, and the corresponding equivalent stiffness is $k = 2734709$ N/m and $k = 2851755$ N/m, respectively. The equivalent damping coefficients calculated based on the experimental measurement results are $c = 1568$ Ns/m and $c = 900$ Ns/m, respectively. The comparison between the vibration transmission rate curve of the equivalent linear vibration isolation system and the experimentally testing results is shown in Fig. 16. The comparison between the test results and the linear damping vibration isolation device shows that the large damping vibration isolation platform proposed in this paper exhibits high damping characteristics at the resonance frequency, which are $c = 1568$ Ns/m and $c = 900$ Ns/m, respectively. When the frequency is lower, the vibration amplitude of the NPR vibration isolator is larger, which causes greater deformation of the damping rubber inside the isolator, and leads to more energy dissipation. Consequently, the effective damping coefficient for the platform with installed mass of $m = 13.55$ kg is greater than that of the equivalent damping coefficient when $m = 4.55$ kg.

When only the energy dissipation relying on the viscoelastic properties of the damping rubber is considered, the comparison between the finite element predictions for the vibration transmissibility of the vibration isolation platform and the experimental testing results is shown in Fig. 17. The magnification of the vibration isolation platform at the resonance predicted by the finite element analysis is greater than that obtained in the experimental testing, and the predicted vibration isolation efficiency at high frequencies is also better than the testing result. Based on the analysis results of the dynamic response of the NPR high damping vibration isolator presented in Section 3, when the energy is only consumed by the viscoelastic characteristics of the damping rubber, the vibration isolation efficiency of the vibration isolator at high frequencies is close to that of undamped vibration isolation system. The comparison between the finite element analysis results and the experimental testing results shown in Fig. 17 approves that, apart from the viscoelastic damping of the rubber, there exists other energy dissipation mechanisms for the NPR vibration isolator. Therefore, the vibration isolation efficiency of the vibration isolation platform at high-frequency slightly decreased in the experimental testing, and in the meantime, the magnification is also reduced at the resonance frequency. In order to verify other possible energy dissipation mechanisms that may exist, Rayleigh damping is set for the negative Poisson's ratio structure in the finite element model with the chosen parameters of $\alpha = 0, \beta = 0.0008$. After setting the additional material damping, the finite element predictions and the experimental testing results on the vibration transmission rate of the vibration isolation platform are compared and shown in Fig. 17. It is observed that the finite element predictions are almost completely consistent with the experimental results.

The comparison results shown in Fig. 17 approved that both of the material damping in the NPR vibration isolator and the viscoelastic properties of the damping rubber have an impact on its vibration transmission rate. Moreover, the material damping will reduce the vibration isolation efficiency of the vibration isolator at high frequencies. In order to achieve a vibration isolator that has low resonant peak and high vibration isolation efficiency simultaneously, the structural material damping of the vibration isolator should be reduced as much as possible, and the resonant peak should be suppressed only by means of the energy dissipation provided by viscoelastic materials. The NPR vibration isolator has many possible parameters that can be optimized, such as the viscoelastic properties of the damping rubber, the Poisson's ratio of the NPR structure, and the stiffness of the NPR structure. The geometry parameters of the NPR vibration isolator in this paper are only chosen by simulation and design experience, and have not been optimized yet. By optimizing the geometric dimensions of the NPR vibration isolator, the resonant peak of the NPR vibration isolator can be further reduced. The main purpose of this paper is to verify the basic design principle and working mechanism of NPR high damping vibration isolator, and demonstrate its *adaptive* damping characteristics and high vibration isolation efficiency. For the optimal design of this proposed NPR high damping vibration isolator, however, it is out of the scope of this paper and will be carried out in our future work.

6. Conclusion

In this paper, by filling viscoelastic damping material inside a negative Poisson's ratio metastructure, a novel vibration isolator with adaptive damping characteristics, simple structural form and small size is proposed, designed and tested. The NPR metastructure can amplify its lateral deformation due to its negative Poisson's ratio effect. As a consequence, the viscoelastic material filled inside the metastructure has enlarged compression and tension along the lateral direction during the vibration process, which makes the viscoelastic rubber dissipate energy more effectively. It, thereby, causes the overall damping characteristics of the vibration isolator to be improved.

The finite element model is first applied to predict the static and dynamic characteristics of the NPR high damping vibration isolator. The hyperelastic and viscoelastic properties of the damping rubber are simulated and characterized based on the 2-parameter Mooney-Rivlin model and the proney series. The static testing results determined the viscoelastic parameters of the damping rubber for the finite element model. The simulation results of the dynamic characteristics of the NPR vibration isolator show that the damping characteristics of the NPR vibration isolator at the resonance frequency are much better than that of the linear spring vibration isolator using the same size damping rubber. At high frequencies, the vibration isolation efficiency of the NPR vibration isolator is close to the undamped linear vibration isolator with the same linear stiffness.

In this paper, a vibration isolation platform based on four NPR vibration isolators is designed and installed for the experimental testing. The vibration transmission rate of the vibration isolation platform is measured through a frequency-sweep testing. The experimental results obtained from the sweep-frequency testing verify the finite element simulation results, and prove that the NPR vibration isolator has high damping characteristics at the resonance frequency and low damping characteristics at the high frequency. This adaptive feature of damping characteristics of a passive vibration isolation system is ideal for applying in precision instruments.

Acknowledgments

The authors sincerely acknowledges the financial support from A3 Talent Researcher Programme of Ningbo University, Zhejiang Province, China.

References

[1] R. Leach, Chapter 3 - precision measurement instrumentation – some design principles, in: R. Leach (Ed.), Fundamental Principles of Engineering Nanometrology (Second Edition), second edition Edition, Micro and Nano Technologies, William Andrew Publishing, Oxford, 2014, pp. 41–61.

[2] E. I. Rivin, Vibration isolation of precision equipment, Precision Engineering 17 (1) (1995) 41–56.

[3] Y. L. Xu, B. Li, Hybrid platform for high-tech equipment protection against earthquake and microvibration, Earthquake engineering & structural dynamics 35 (8) (2006) 943–967.

[4] C. Liu, X. Jing, S. Daley, F. Li, Recent advances in micro-vibration isolation, Mechanical Systems and Signal Processing 56 (2015) 55–80.

[5] G. Yan, H.-X. Zou, S. Wang, L.-C. Zhao, Z.-Y. Wu, W.-M. Zhang, Bio-inspired vibration isolation: methodology and design, Applied Mechanics Reviews 73 (2) (2021) 020801.

[6] G. L. Hermsdorf, S. A. Szilagyi, S. Rösch, E. Schäffer, High performance passive vibration isolation system for optical tables using six-degree-of-freedom viscous damping combined with steel springs, Review of Scientific Instruments 90 (1) (2019) 015113.

[7] L. Li, L. Wang, L. Yuan, R. Zheng, Y. Wu, J. Sui, J. Zhong, Micro-vibration suppression methods and key technologies for high-precision space optical instruments, Acta Astronautica (2020).

[8] G. Aglietti, R. Langley, E. Rogers, S. Gabriel, Model building and verification for active control of microvibrations with probabilistic assessment of the effects of uncertainties, Proceedings of the Institution of Mechanical Engineers, Part C: Journal of Mechanical Engineering Science 218 (4) (2004) 389–399.

[9] M. Rafiee, F. Nitzsche, M. Labrosse, Dynamics, vibration and control of rotating composite beams and blades: A critical review, Thin-Walled Structures 119 (2017) 795–819.

[10] J. C. Snowdon, Vibration isolation: use and characterization, The Journal of the Acoustical Society of America 66 (5) (1979) 1245–1274.

[11] R. Ibrahim, Recent advances in nonlinear passive vibration isolators, Journal of sound and vibration 314 (3-5) (2008) 371–452.

[12] K. Ghaedi, Z. Ibrahim, H. Adeli, A. Javanmardi, Invited review: Recent developments in vibration control of building and bridge structures, Journal of Vibroengineering 19 (5) (2017) 3564–3580.

[13] A. Agrawal, M. Amjadian, Chapter 20 - seismic component devices, in: A. Pipinato (Ed.), Innovative Bridge Design Handbook, Butterworth-Heinemann, Boston, 2016, pp. 531–553.

[14] R. Rana, T. Soong, Parametric study and simplified design of tuned mass dampers, Engineering structures 20 (3) (1998) 193–204.

[15] R. I. Skinner, J. M. Kelly, A. Heine, Hysteretic dampers for earthquake-resistant structures, Earthquake Engineering & Structural Dynamics 3 (3) (1974) 287–296.

[16] J. Ji, Q. Luo, K. Ye, Vibration control based metamaterials and origami structures: A state-of-the-art review, Mechanical Systems and Signal Processing 161 (2021) 107945.

[17] X. Zheng, H. Lee, T. H. Weisgraber, M. Shusteff, J. DeOtte, E. B. Duoss, J. D. Kuntz, M. M. Biener, Q. Ge, J. A. Jackson, et al., Ultralight, ultrastiff mechanical metamaterials, Science 344 (6190) (2014) 1373–1377.

[18] H. Huang, C. Sun, G. Huang, On the negative effective mass density in acoustic metamaterials, International Journal of Engineering Science 47 (4) (2009) 610–617.

[19] G. Hu, L. Tang, J. Xu, C. Lan, R. Das, Metamaterial with local resonators coupled by negative stiffness springs for enhanced vibration suppression, Journal of Applied Mechanics 86 (8) (2019) 081009.

[20] K. K. Saxena, R. Das, E. P. Calius, Three decades of auxetics research-materials with negative poisson's ratio: a review, Advanced Engineering Materials 18 (11) (2016) 1847–1870.

[21] K. Liu, L. Han, W. Hu, L. Ji, S. Zhu, Z. Wan, X. Yang, Y. Wei, Z. Dai, Z. Zhao, et al., 4d printed zero poisson's ratio metamaterial with switching function of mechanical and vibration isolation performance, Materials & Design 196 (2020) 109153.

[22] Q. Wang, J. A. Jackson, Q. Ge, J. B. Hopkins, C. M. Spadaccini, N. X. Fang, Lightweight mechanical metamaterials with tunable negative thermal expansion, Physical review letters 117 (17) (2016) 175901.

[23] R. Zhu, X. Liu, G. Hu, C. Sun, G. Huang, A chiral elastic metamaterial beam for broadband vibration suppression, Journal of Sound and Vibration 333 (10) (2014) 2759–2773.

[24] Q. Zhang, D. Guo, G. Hu, Tailored mechanical metamaterials with programmable quasi-zero-stiffness features for full-band vibration isolation, Advanced Functional Materials (2021) 2101428.

[25] C. Morris, L. Bekker, C. Spadaccini, M. Haberman, C. Seepersad, Tunable mechanical metamaterial with constrained negative stiffness for improved quasi-static and dynamic energy dissipation, Advanced Engineering Materials 21 (7) (2019) 1900163.

[26] H. Fan, L. Yang, Y. Tian, Z. Wang, Design of metastructures with quasi-zero dynamic stiffness for vibration isolation, Composite Structures 243 (2020) 112244.

[27] S. Sadeghi, S. Li, Harnessing the quasi-zero stiffness from fluidic origami for low frequency vibration isolation, in: Smart Materials, Adaptive Structures and Intelligent Systems, Vol. 58264, American Society of Mechanical Engineers, 2017, p. V002T03A008.

[28] C. Cai, J. Zhou, L. Wu, K. Wang, D. Xu, H. Ouyang, Design and numerical validation of quasi-zero-stiffness metamaterials for very low-frequency band gaps, Composite structures 236 (2020) 111862.

[29] C. Li, T. Jiang, Q. He, Z. Peng, Stiffness-mass-coding metamaterial with broadband tunability for low-frequency vibration isolation, Journal of Sound and Vibration 489 (2020) 115685.

[30] Z. Wang, Q. Zhang, K. Zhang, G. Hu, Tunable digital metamaterial for broadband vibration isolation at low frequency, Advanced materials 28 (44) (2016) 9857–9861.

[31] Z.-D. Xu, Y.-P. Shen, H.-T. Zhao, A synthetic optimization analysis method on structures with viscoelastic dampers, Soil Dynamics and Earthquake Engineering 23 (8) (2003) 683–689.

[32] J. Kim, J. Ryu, L. Chung, Seismic performance of structures connected by viscoelastic dampers, Engineering Structures 28 (2) (2006) 183–195.

[33] A. Lago, D. Trabucco, A. Wood, Case studies of tall buildings with dynamic modification devices, Damping Technologies for Tall Buildings (2018).

[34] C. D. Johnson, D. A. Kienholz, Finite element prediction of damping in structures with constrained viscoelastic layers, AIAA journal 20 (9) (1982) 1284–1290.

[35] B. Samali, K. Kwok, Use of viscoelastic dampers in reducing wind-and earthquake-induced motion of building structures, Engineering Structures 17 (9) (1995) 639–654.

[36] A. Baz, Damping, active, in: S. Braun (Ed.), Encyclopedia of Vibration, Elsevier, Oxford, 2001, pp. 351–364.

[37] E. H. Anderson, R. M. Glaese, D. Neill, A comparison of vibration damping methods for ground based telescopes, in: Ground-based and Airborne Telescopes II, Vol. 7012, International Society for Optics and Photonics, 2008, p. 70120H.

[38] M. Mehrabi, M. Suhatril, Z. Ibrahim, S. Ghodsi, H. Khatibi, Modeling of a viscoelastic damper and its application in structural control, PloS one 12 (6) (2017) e0176480.

[39] M. Ye, L. Gao, H. Li, A design framework for gradually stiffer mechanical metamaterial induced by negative poisson's ratio property, Materials & Design 192 (2020) 108751.

[40] X.-W. Zhang, D.-Q. Yang, Numerical and experimental studies of a light-weight auxetic cellular vibration isolation base, Shock and Vibration 2016 (2016).

[41] N. Shedbale, P. Muley, Review on viscoelastic materials used in viscoelastic dampers, International Research Journal of Engineering and Technology 1 (2017).

[42] A. U. Manual, Abaqus user manual, Abacus (2020).

[43] Q. Zhang, Y. Peng, Q. Ai, Y. Xiao, Comparison of two methods on determining the parameters of mooney rivlin model for rubber based on abaqus, Special Purpose Rubber Products 38 (6) (2017) 52–54.

[44] R. E. Blake, Basic vibration theory, Shock and vibration handbook 1 (1961) 2–8.

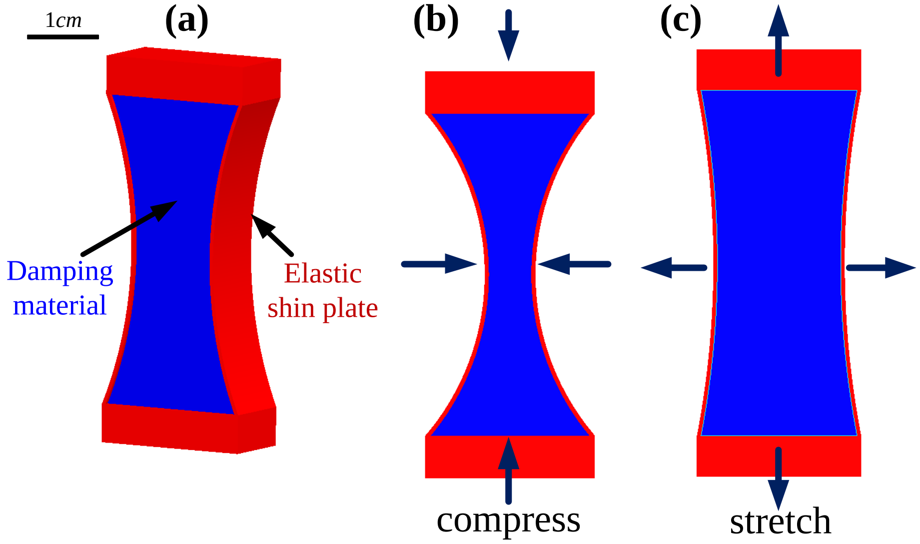

Figure 1: A unit cell with negative Poisson's ratio

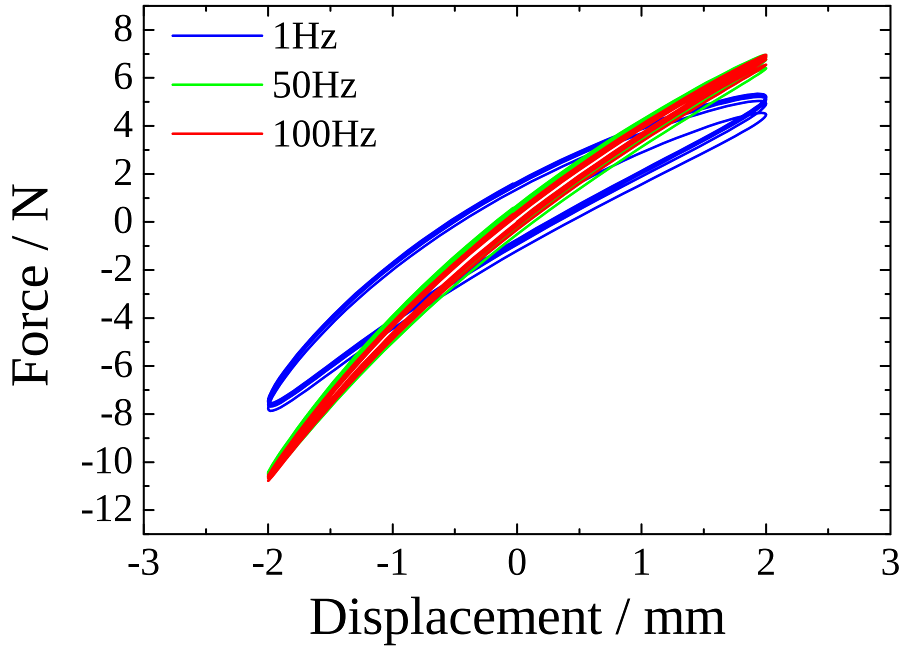

Figure 2: Unixial force-displacement curve of a $10mm^3$ rubber cube

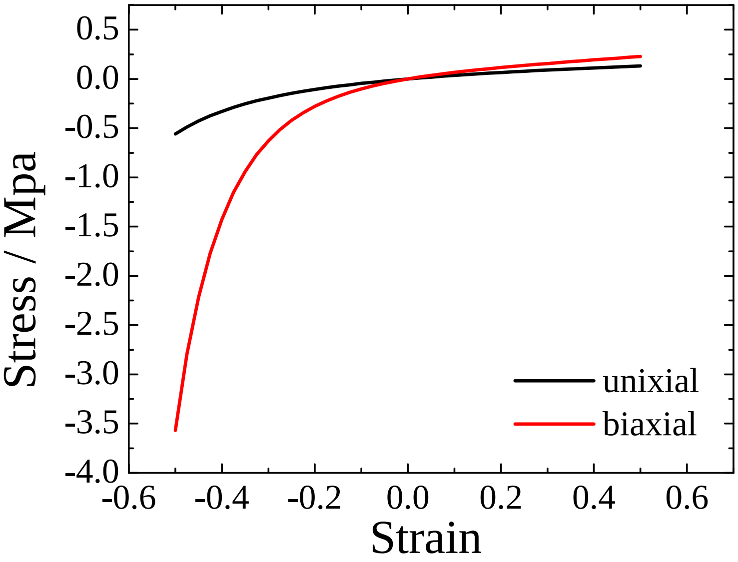

(a) The stress-strain curve

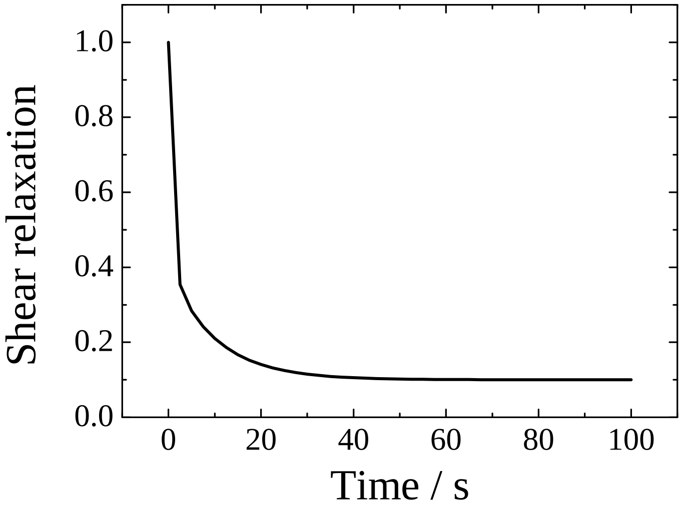

(b) The stress relaxation curve

Figure 3: Mechanical property of butyl rubber

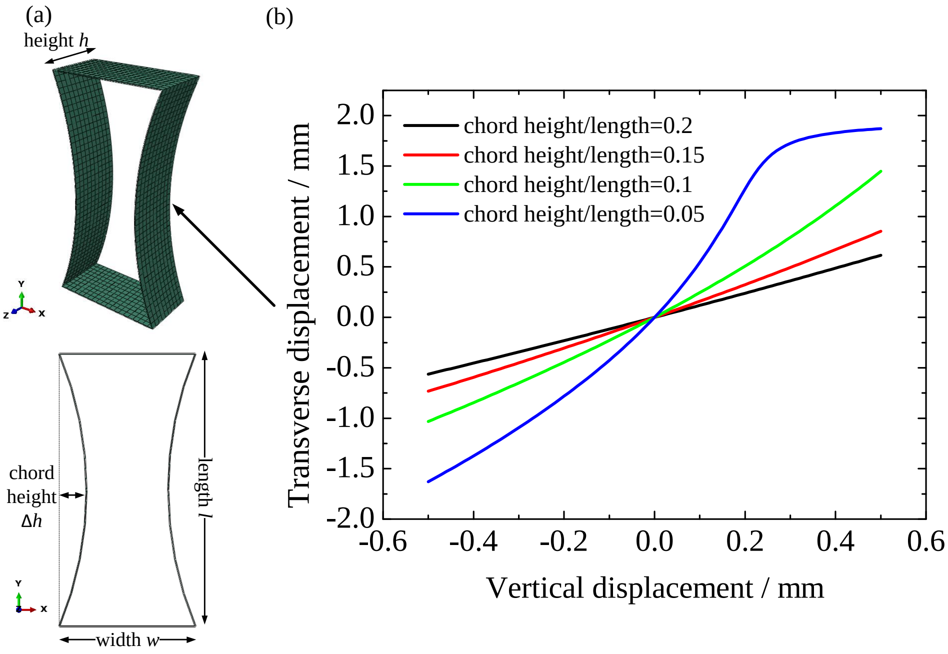

Figure 4: Deforming response of the negative Poisson's ratio structure. (a)Finite element model(b)Variation of transverse deformation along with the vertical deformation

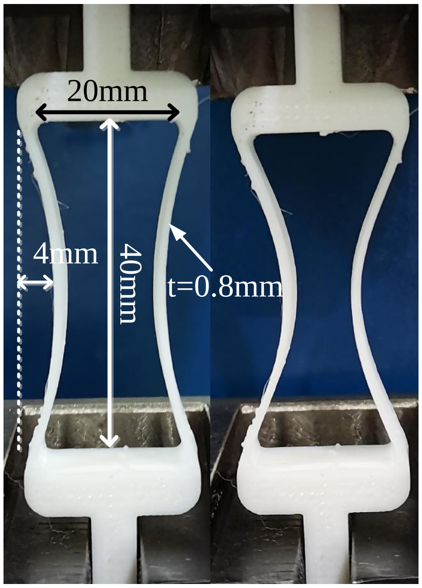

(a) Experimental settlement

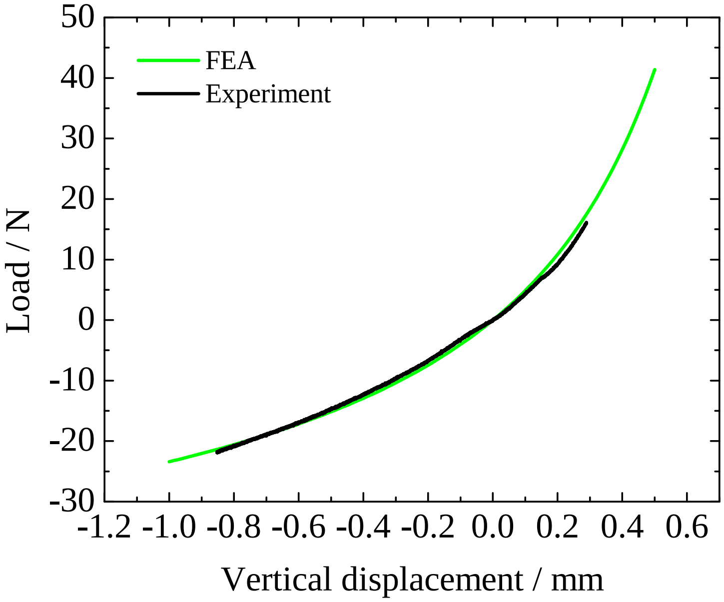

(b) Load-displacement curves

Figure 5: Tensile test of a 3D-printed metastructure unit

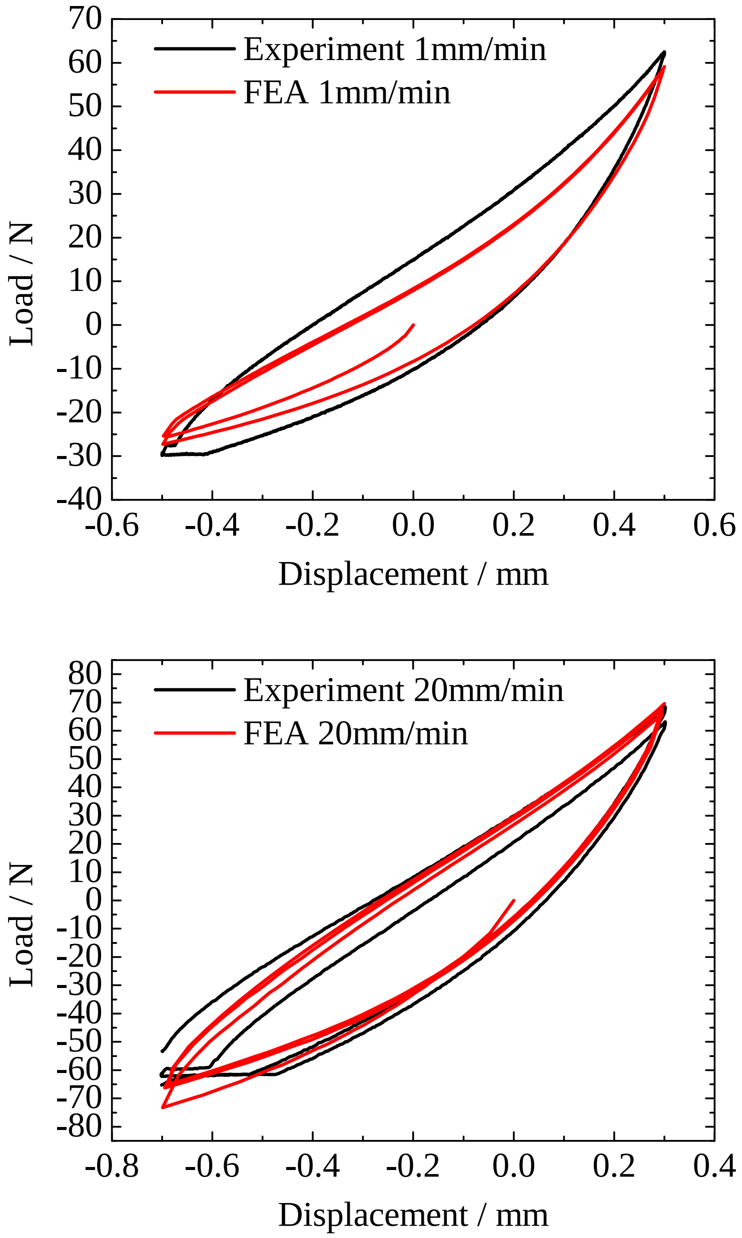

Figure 6: Hysteresis curves of the vibration isolator

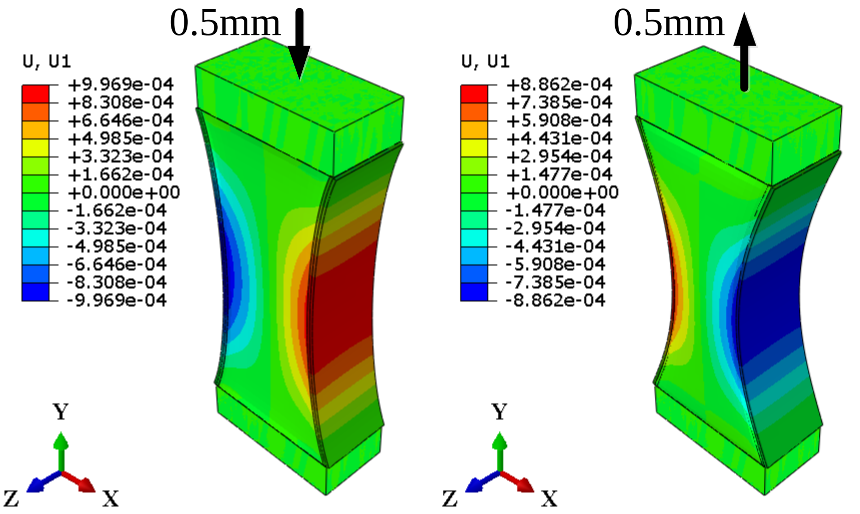

(a) With NPR metastructure

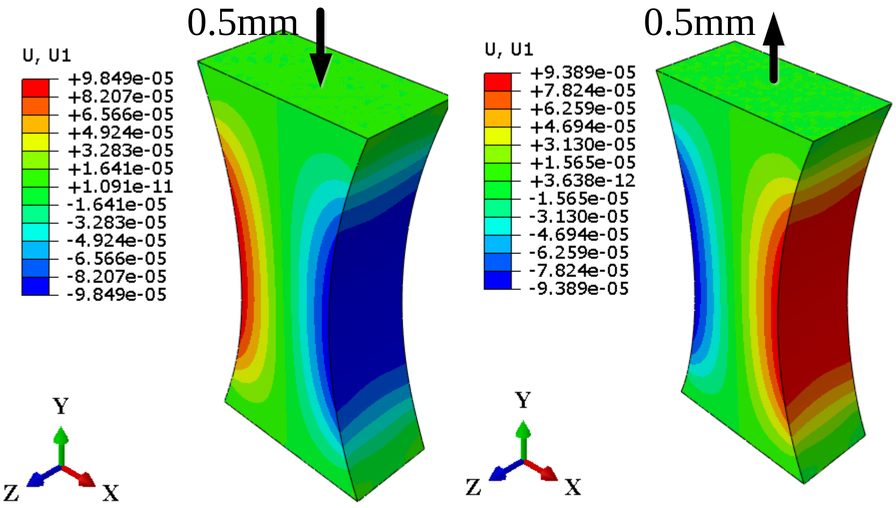

(b) Without NPR metastructure

Figure 7: Lateral deformation contour maps of butyl rubbers

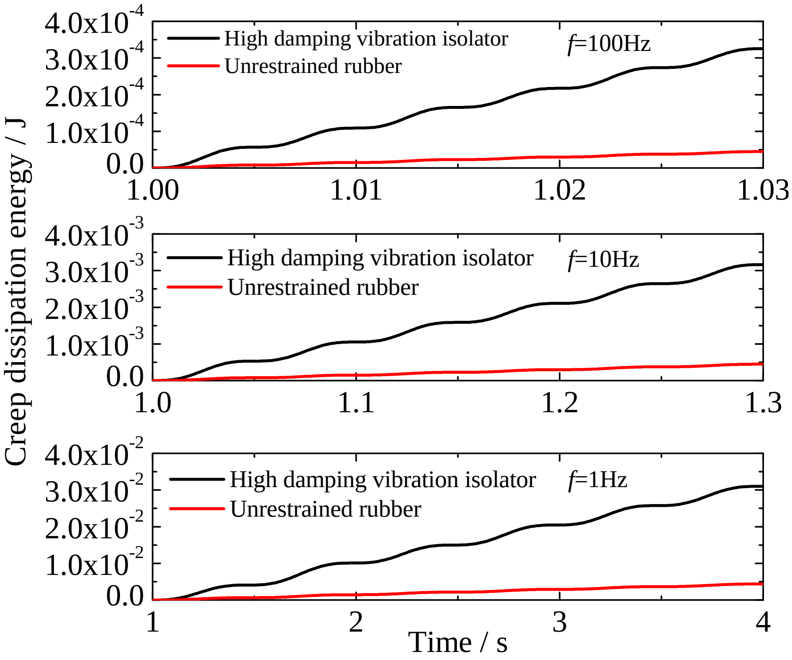

Figure 8: Creep dissipation energy curves of the damping butul rubbers with and without the constraint of the NPR metastructure

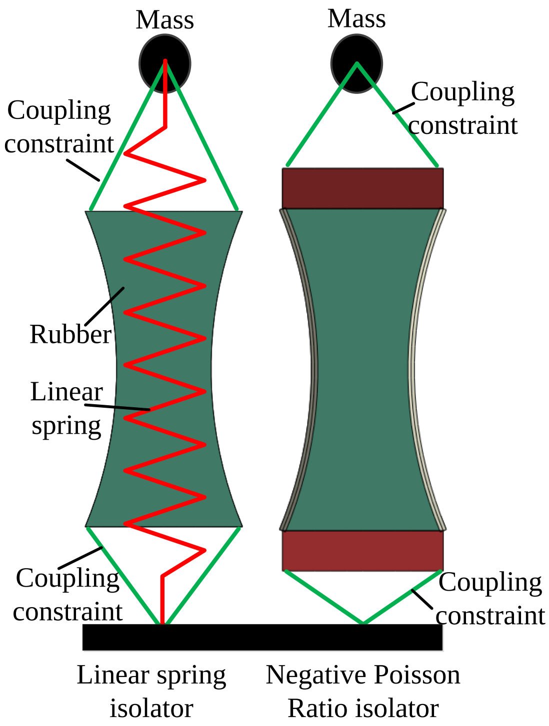

(a) Illustration for the finite element model of the two isolators

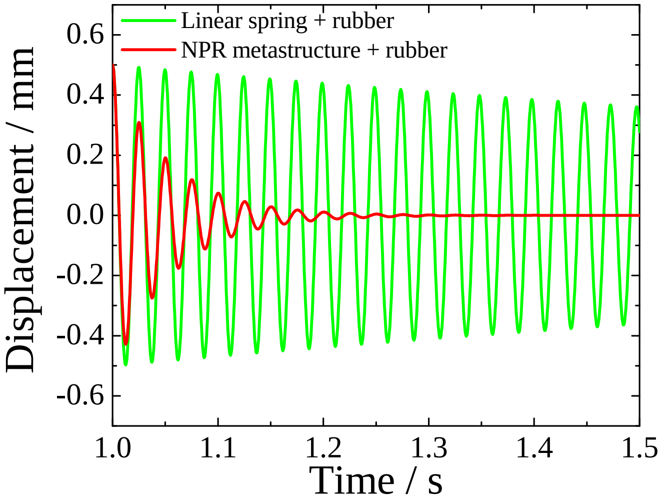

(b) Predicted displacement osillation curves of the free vibration

Figure 9: Illustration of the linear spring vibration isolator and the high damping vibration isolator, and the simulated responses of free vibration

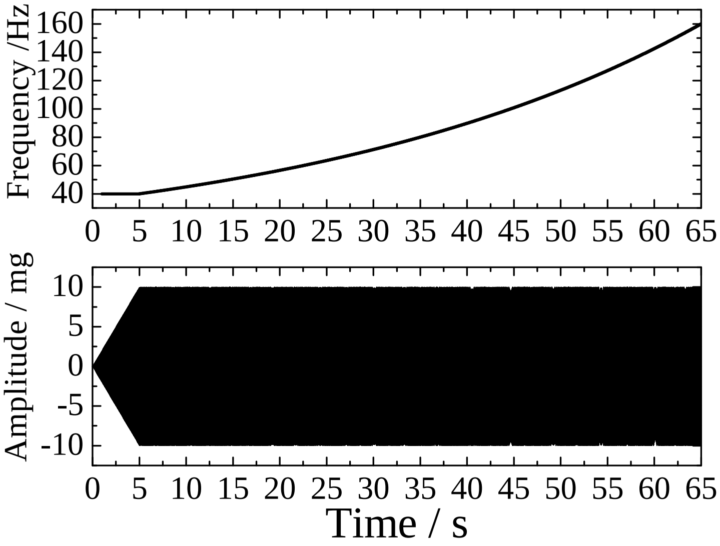

Figure 10: Sweep excitation applied in the dynamic response analysis

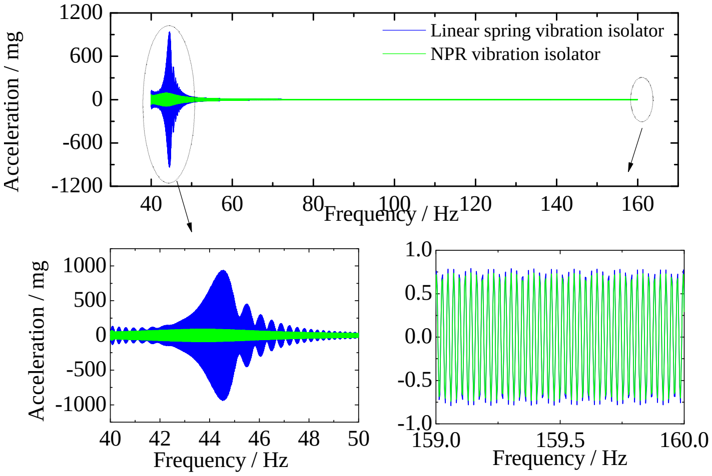

(a) $m = 10\text{Kg}$

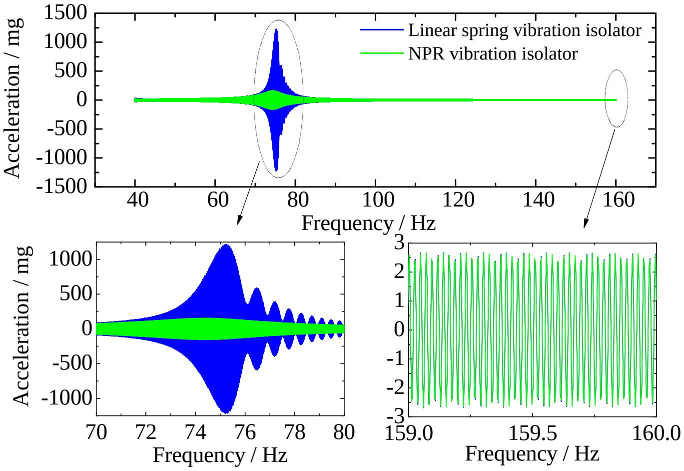

(b) $m = 3.3875\text{Kg}$

Figure 11: Response comparison of the linear spring vibration isolator and the NPR vibration isolator under the Sweep excitation

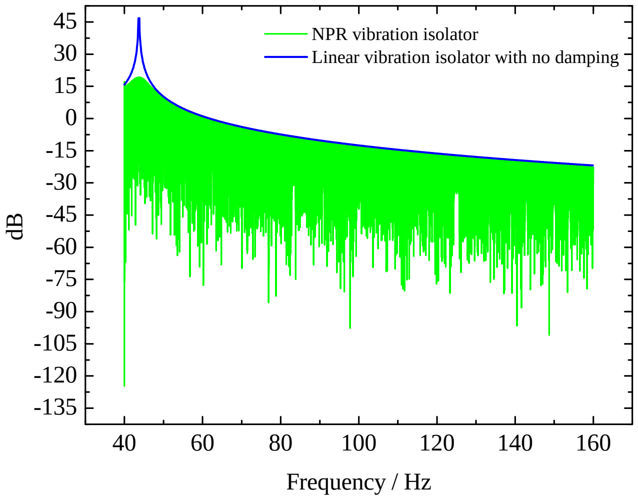

(a) $m = 10\text{Kg}$

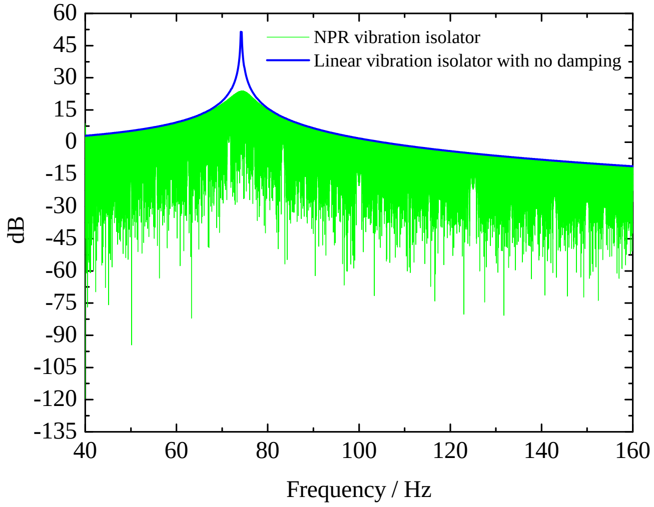

(b) $m = 3.3875\text{Kg}$

Figure 12: Transmissity comparison of a undamped linear vibration isolator and the NPR vibration isolator

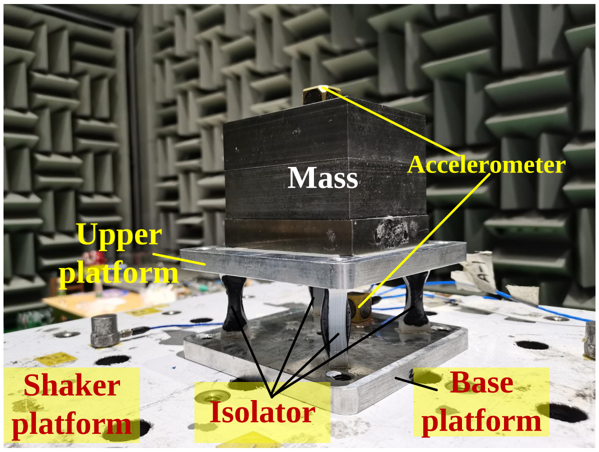

Figure 13: Vibration isolating platform with 4 NPR vibration isolators

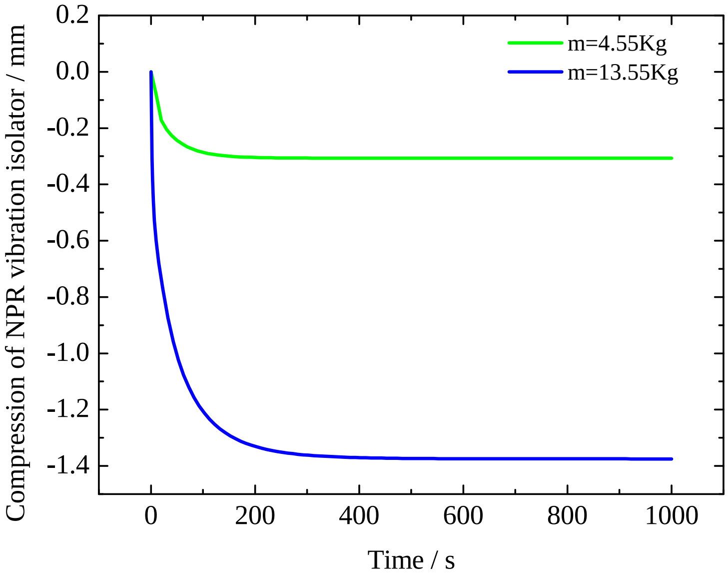

Figure 14: Vertical compression of NPR vibration isolators as result of gravity

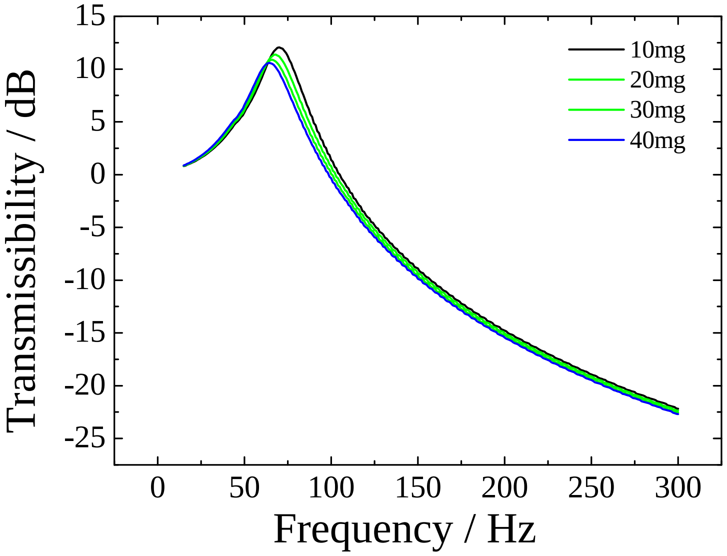

(a) Total Mass m = 13.55 kg

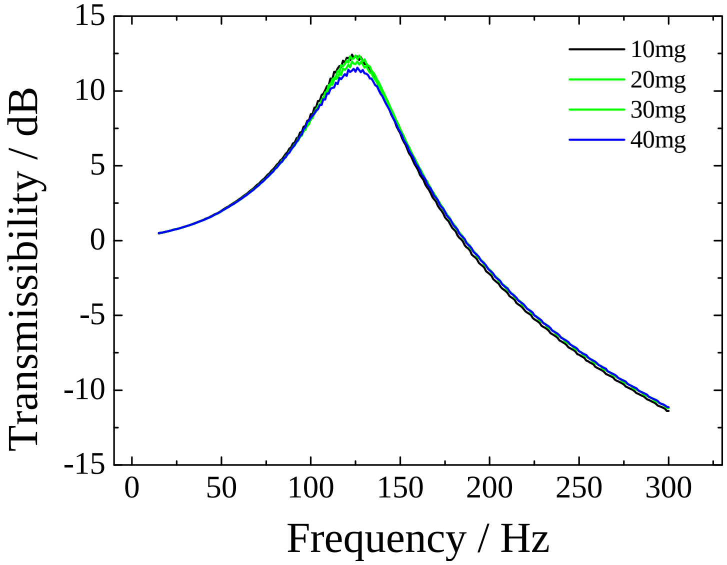

(b) Total Mass m = 4.55 kg

Figure 15: Experimental results (Transmissibility *vs.* Frequency) from the frequency-sweep testing of vibration isolation platform.

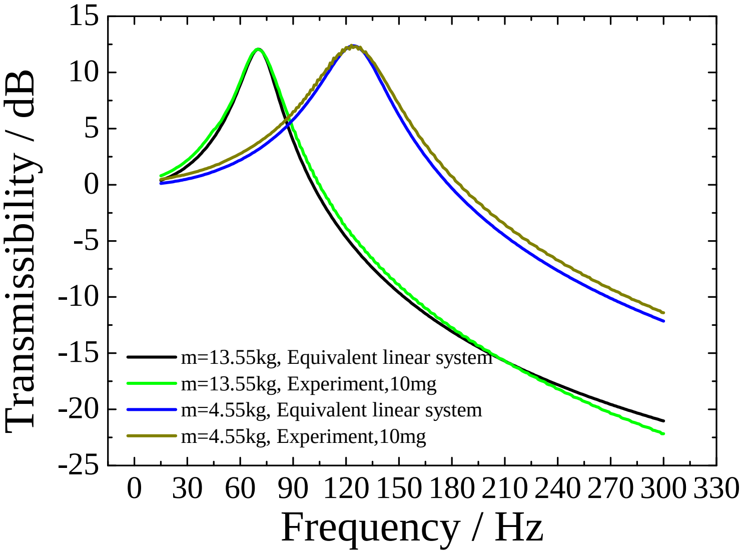

Figure 16: Comparison of the vibration transmission rate between the experimental testing results of the vibration isolation platform and the equivalent linear vibration isolation system

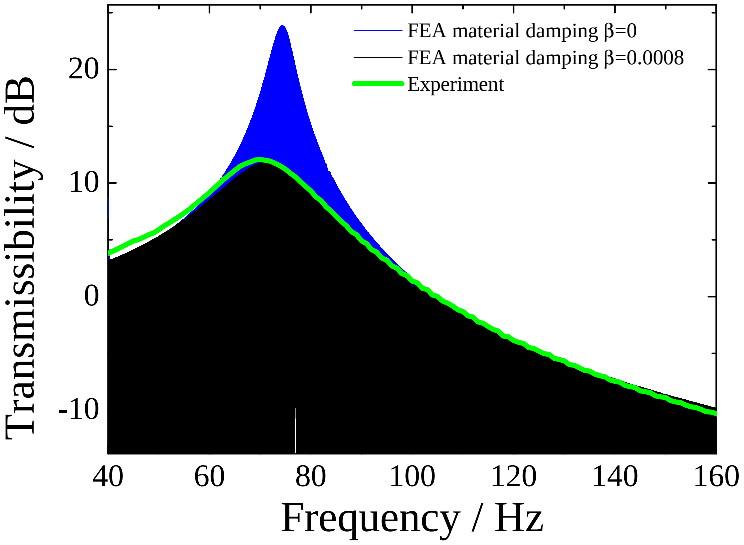

Figure 17: Comparison of experimental results and Finite Element predictions on the transmissibility of NPR vibration isolator